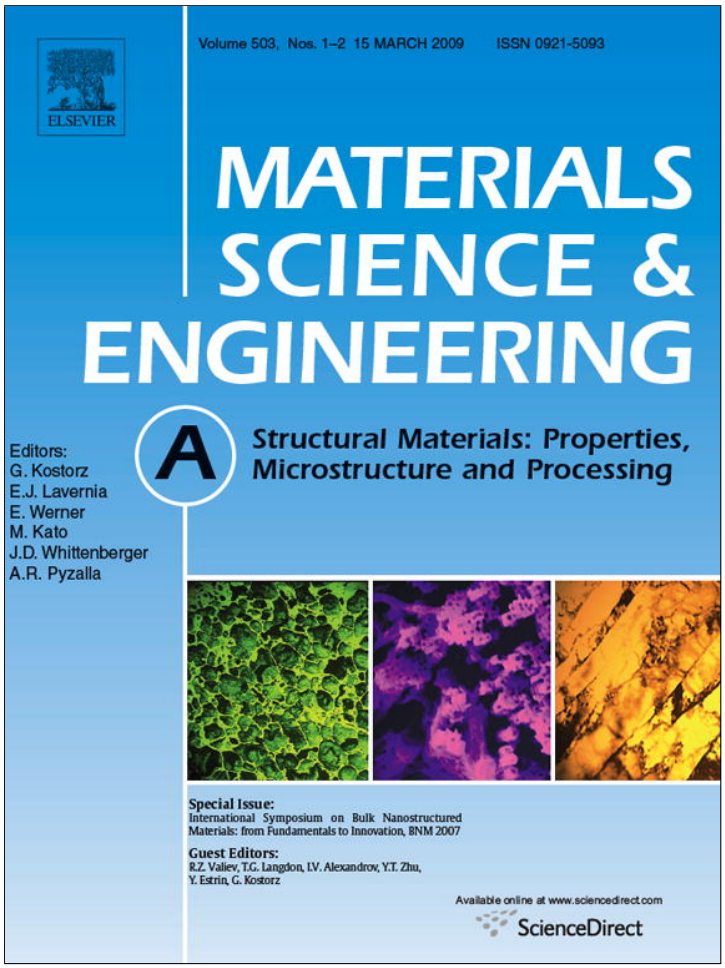

Materials Science and Engineering A 503 (2009) 185–189

Contents lists available at ScienceDirect

Materials Science and Engineering A

journal homepage: www.elsevier.com/locate/msea

Fe–C nanograined alloys obtained by high-pressure torsion: Structure and magnetic properties

B.B. Straumal[a,b,*], A.A. Mazilkin[b], S.G. Protasova[b], S.V. Dobatkin[c], A.O. Rodin[d], B. Baretzky[a], D. Goll[a], G. Schütz[a]

[a] Max-Planck-Institut für Metallforschung, Heisenbergstrasse 3, 70569 Stuttgart, Germany
[b] Institute of Solid State Physics, Russian Academy of Sciences, Chernogolovka, Moscow District 142432, Russia
[c] A.A. Baikov Institute of Metallurgy and Materials Science, Russian Academy of Sciences, Leninsky Prosp. 49, Moscow 119991, Russia
[d] Moscow State Institute of Steel and Alloys (Technological University), Leninsky Prosp. 4, Moscow 119991, Russia

ARTICLE INFO

Article history:
Received 20 January 2008
Received in revised form 26 February 2008
Accepted 1 March 2008

Keywords:
High-pressure torsion
Nanograined structure
Fe–C alloys
Light microscopy
Electron microscopy
Mössbauer spectroscopy
Magnetic properties

ABSTRACT

The microstructure, phase composition, Mössbauer spectra and magnetic properties of nine binary Fe–C alloys with carbon concentrations between 0.05 and 1.7 wt.% were studied in the as-cast state, after a long annealing at 725 °C and after high-pressure torsion (HPT) at ambient temperature and 5 GPa with five anvil rotations (shear strain about 6). The grain size after HPT was in the nanometer range. Only Fe_3C (cementite) and α-Fe remain in the alloys after HPT. It was also shown that the less stable Hägg carbide (Fe_5C_2) and retained austenite disappear, and phase composition closely approaches the equilibrium corresponding to the HPT temperature and pressure. Measurements of saturation magnetization and Mössbauer effect reveal that the amount of cementite decreases after HPT. The reason for partial cementite dissolution is the formation of the carbon-rich segregation layers in the ferrite grain boundaries.

1. Introduction

The unique properties of the nanostructured materials are of great importance for various advanced applications. Comprehensive investigation of nanograined polycrystals is crucial especially for the alloys, which are most important for technological use. Iron–carbon system plays a fundamental role in structural applications. The most important methods for preparing nanograined polycrystals are gas condensation, crystallization from amorphous state, ball milling and severe plastic deformation (SPD) techniques. SPD techniques, such as equal-channel angular pressing (ECAP) and high-pressure torsion (HPT) do not involve changes in the material geometry, in contrast to the conventional processes of high deformation like rolling or wire drawing [1–4].

It has been shown recently that HPT causes grain refinement and decomposition of a supersaturated solid solution [3,4]. The phase composition closely approaches the equilibrium state at SPD pressure and temperature. It has been concluded that SPD can be considered as "hot deformation at room temperature", i.e. a balance between deformation-induced grain refinement and deformation-accelerated formation of equilibrium phases. The Fe–C system is very rich on the stable and metastable phases. SPD can lead to their spectacular evolution. One of these processes reported in a number of experimental works is the paradoxial cementite dissolution [1,2,5–9]. The aim of this study was to investigate thoroughly structural changes in Fe–C alloys during HPT in a broad interval of carbon concentration and to resolve the question of cementite disappearance during the SPD processing of the material.

2. Experimental

Both hypo- and hypereutectoid Fe–C alloys with carbon concentrations of 0.05, 0.10, 0.20, 0.25, 0.45, 0.60, 1.3, 1.5 and 1.7 wt.% were prepared from high-purity 5N Fe and C by vacuum induction melting in the form of cylindrical 12-mm-diameter ingots. The carbon content was measured by atomic absorption spectroscopy in a PerkinElmer spectrometer. Two-millimeter-thick discs were cut from the cast ingots in order to investigate the as-cast state. For HPT treatment 0.4-mm-thick discs were cut from the cast ingots, then ground and chemically etched. They were subjected to HPT at

* Corresponding author at: Institute of Solid State Physics, Russian Academy of Sciences, Chernogolovka, Moscow District 142432, Russia. Tel.: +7 49652 22957; fax: +7 49652 49701.
E-mail address: straumal@issp.ac.ru (B.B. Straumal).

0921-5093/$ – see front matter © 2008 Published by Elsevier B.V.
doi:10.1016/j.msea.2008.03.052

room temperature in a Bridgman anvil-type unit under a pressure of 5 GPa and for 5 torsions. Shear strain was about 6. Samples for structural and magnetic investigations were cut from the HPT-deformed discs at a distance of 3 mm from the sample center. One set of as-cast samples with 0.25, 0.60, 1.3 and 1.7 wt.% C was additionally annealed for 950 h at 725 °C (i.e. below the eutectoid temperature) in order to achieve the equilibrium $\alpha + Fe_3C$ structure. Light microscopy (LM) was performed with Zeiss Axiophot microscope. For the metallographic investigations the samples were ground by SiC grinding paper, polished with 6, 3 and 1 μm diamond pastes and etched for 5–10 s with a 5 wt.% HNO_3 solution in ethyl alcohol. Transmission electron microscopy (TEM) investigations were carried out on a JEM–4000FX microscope at accelerating voltage of 400 kV. X-ray diffraction (XRD) data were obtained on Siemens diffractometer (Co Kα radiation). XRD spectra were measured in a short 2θ interval (30–70°) with fine angular step of 0.04° and the intensity was collected for 30 s in each point. As a result the signal/noise ratio was above 2 even for the very weak peaks of iron carbides. Calculation of the grain or particle size (D) from the X-ray peak broadening was done using the Scherer's formula: $D = 0.9\lambda/\beta\cos\theta$, where λ is the X-ray wavelength, θ is the diffraction angle and β is the full-width at half maximum of the diffraction line.

Magnetic measurements were performed in a vibrating sample magnetometer (VSM). Discs of 3 mm diameter and 0.15 mm thickness were cut for the magnetic investigations. The magnetic field in VSM was applied parallel to the sample plane. Mössbauer experiments were performed using a Perseus spectrometer with Co^{57} source in the rhodium matrix at room temperature in the velocity interval from −10 to 10 mm/s with 256 registration channels. It allowed defining the effective magnetic field with an error of less than 5 kOe. Spectra were analyzed using the less square method for the superposition of Lorentz lines corresponding to the absorption of various phases. Auger-electron spectroscopy (AES) of HPT Fe–1.7 wt.% C alloys was performed using a PHI 680 Auger spectrometer. After HPT the samples became rather brittle and were broken *in situ* in the spectrometer chamber. The spectra resulting from the fracture surfaces immediately after the cleavage contained oxygen, carbon and iron peaks. Oxygen peaks disappeared after about 60 s of ion etching; the carbon concentration also decreased within this period and then remained at a low but constant level during further etching.

3. Results

The lattice parameter of the α-Fe solid solution in samples after HPT is about 0.28667 ± 0.3 nm and does not depend on the total carbon concentration in the alloys. This is about 4×10^{-5} nm higher than that for pure α-Fe (0.28664 nm [10]). The addition of 0.018 wt.% C to pure α-Fe (being the solubility of carbon in α-Fe at 680 °C [11]) increases the lattice parameter of α-Fe by 7×10^{-5} nm [12]. This means that the carbon concentration in α-Fe after HPT is about 0.01 wt.% C. It does not exceed the carbon maximum solubility (about 0.02 wt.% at 740 °C). Within the framework of experimental error, it more or less corresponds to the solubility at room temperature [11]. In other words, HPT does not lead to the formation of supersaturated carbon solid solution in the bulk of α-Fe grains. XRD reveals that both hypoetectoid and hypereutectoid Fe–C alloys do not contain martensite (i.e. body-centered tetragonal supersaturated solid solution of carbon in α-Fe), since the splitting of (2 0 0) line typical for tetragonal martensite lattice was not observed either before or after HPT.

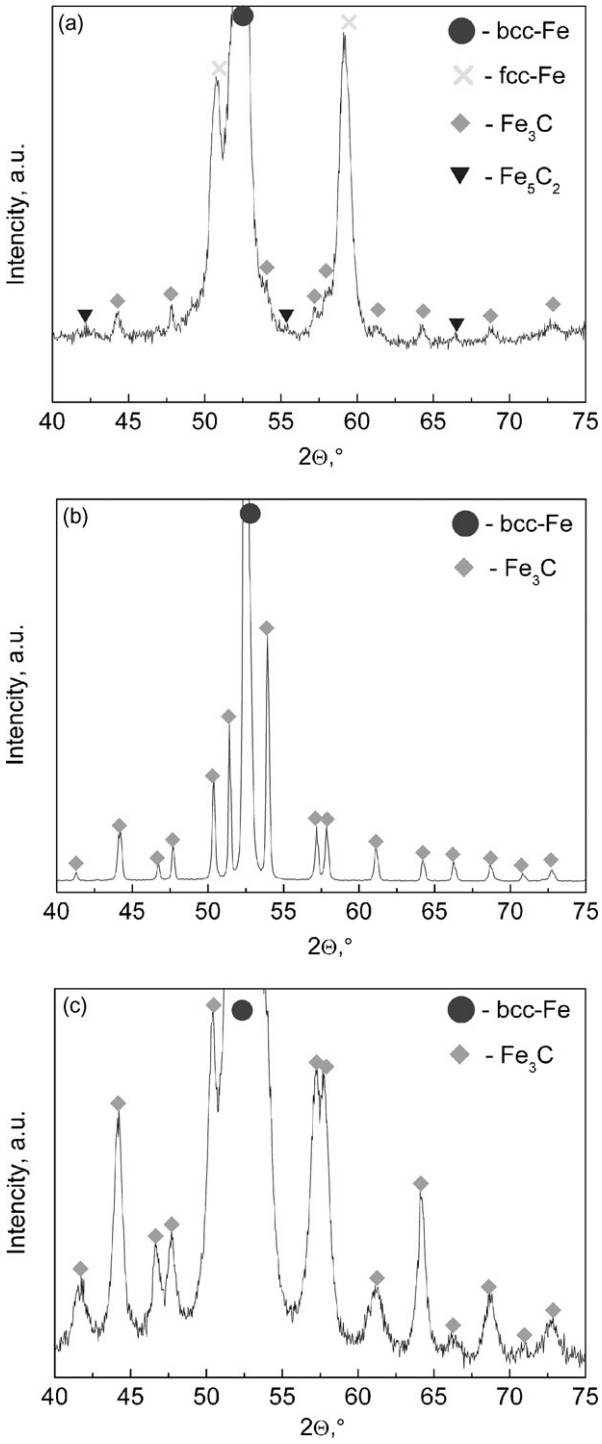

Fig. 1. X-ray diffraction spectra for the Fe–1.7 wt.% C alloy. (a) Initial as-cast alloy. (b) After annealing at 725 °C, 950 h. (c) After HPT at 5 GPa, 5 torsions. (1 1 0) ferrite peak is marked by a filled circle. Crosses mark the retained austenite. Filled diamonds mark the peaks of cementite Fe_3C.

In Fig. 1a–c the XRD spectra are shown for the Fe–1.7 wt.% C alloy. The initial as-cast alloy (Fig. 1a) contains three phases. First, a strong peak of α-Fe with body-centered cubic (bcc) lattice is present (marked by a filled circle). This peak ($2\theta = 52.48°$) is slightly shifted from the pure Fe position due to the diluted carbon atoms, as discussed above. Second, peaks of retained austenite (face-centered cubic, γ-Fe) are detected (marked by crosses). Third, rather weak and broadened peaks of cementite are also present (marked by

filled diamonds). Some very weak peaks (like those at $2\theta = 42.23^\circ$, 55.3°, and 66.48°) can be attributed as diffraction from the Hägg carbide Fe_5C_2. Fig. 1b contains the data for the Fe–1.7 wt.% C alloy annealed during 950 h at 725 °C in the α + Fe_3C two-phase region of the Fe–C phase diagram. The spectrum contains only two phases, namely, ferrite and cementite. All peaks are well separated from each other and very narrow, much narrower than those in the as-cast state. It means that after a very long annealing both ferrite and cementite grains became large and crystallographically perfect. No peaks of retained austenite and Hägg carbide are present. Fig. 1c contains the diffraction spectrum for the Fe–1.7 wt.% C alloy after HPT. Similar to the results in Fig. 1b, only two phases (ferrite and cementite) remained after HPT in the sample and retained austenite, and Hägg carbide disappeared. However, all peaks are broadened even in comparison with the as-cast state. This fact witnesses that the fine grain size and/or residual stresses are present in samples after HPT. Similar results were obtained also in the hypoeutectoid Fe–0.6 wt.% C alloy. Only the quantity of iron carbides, according to the phase diagram, was 3 times lower than in the Fe–1.7 wt.% C alloy. Therefore, the intensity of all cementite peaks was also comparatively lower. The size of the cementite particles after HPT measured from the data on X-ray peak broadening was ~25–30 nm. XRD did not show any presence of graphite in all studied samples.

It has to be underlined that the observed fine structure of the XRD spectra was detectable only due to fine angular steps and high counting statistics. If one would investigate the X-ray diffraction in conventional conditions and compare the as-cast and HPT alloys, one would come to the erroneous conclusions, that (a) only ferrite and retained austenite are present in the as-cast state, and (b) after HPT retained austenite disappeared without formation of cementite.

LM investigations of the hypoeutectoid (i.e. below 0.8 wt.% C) as-cast alloys reveal that the following structural components are present: (i) the austenite grains transformed into ferrite + austenite mixture during cooling through the ferrite + austenite region of the Fe–C phase diagram; (ii) initial austenite plates transformed into perlite or troostite; (iii) the ferrite layers along grain boundaries (GBs) of transformed austenite (primary ferrite) [13,14]. The microstructures of hyperetectoid alloys are similar to each other, but differ from those of hypoetectoid alloys [13,14]. They contain the initial austenite grains transformed into troostite which appears grey. GBs between former austenite grains are covered by the cementite layers. They were most probably formed by cooling in two phase austenite + cementite region of the Fe–C phase diagram. The Widmanstätten plates growing from GB cementite are visible. The amount of primary cementite (and also the number of cementite Widmanstätten plates) increases with increasing carbon content.

The bright field TEM image of the coarse grained as-cast Fe–C alloys and respective selected area electron diffraction (SAED) pattern revealed that transformed austenite grains contained the troostite lamellar colonies with interlamellar spacing of 100–400 nm [13,14]. TEM of the as-cast alloys with 0.25, 0.45, 0.60, 1.3, and 1.5 wt.% C revealed the presence of ferrite, cementite and retained austenite in all studied alloys. Only the amount of these phases is different in various alloys, in conformity with Fe–C phase diagram [15]. The amount of Hägg carbide in the as-cast alloys is very small; the respective diffraction spots are not present in all studied locations. According to the LM and TEM, the grain size of ferrite (in hypoeutectoid alloys), retained and transformed austenite (in all alloys) scattered from 200 to 700 μm. TEM and LM also do not show any presence of martensite in the as-cast state of material. Neither split (2 0 0) spots (typical for tetragonal martensite lattice) in the SAED patterns nor typical for martensite grain morphology

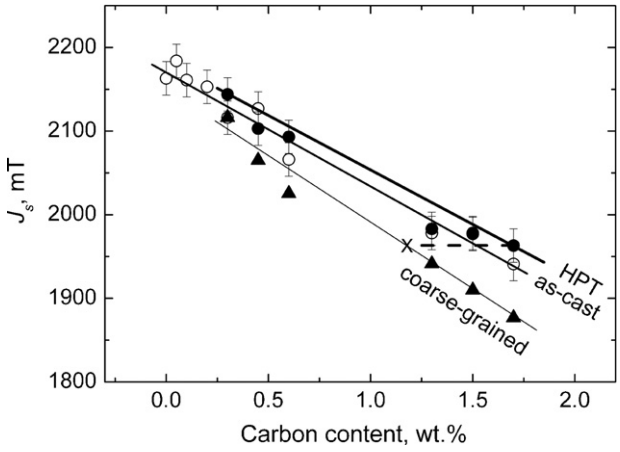

Fig. 2. Dependence of saturation magnetization J_s on carbon concentration for as-cast and HPT-treated alloys.

(needles, plates) were discovered in LM. Electron diffraction, similar to XRD did not show any presence of graphite in all samples studied.

The structures of hypoeutectoid and hypereutectoid alloys became very similar after long annealing for 950 h at 725 °C (i.e. below the eutectoid temperature) [13,14]. All samples contain very coarse ferrite and cementite grains. Only the amount of cementite is different which increases with increasing carbon content, according to the Fe–C phase diagram [15].

Nanometer range grain structure is obtained in the alloys as a result of the severe plastic deformation by HPT [13,14]. SAED patterns contain only α-Fe and Fe_3C spots. The TEM micrographs and SAED patterns of Fe alloys with 0.45, 0.60, 1.3, 1.5 and 1.7 wt.% C after HPT are very similar. Both the ferrite grains and cementite particles are visible in the dark field images as the reflections of these phases lie closely to each other. Dislocation density is $>10^{14}$ m^{-2} in all samples. Ferrite grain size after HPT is about 100 nm. It increases slightly with increasing carbon content. Ferrite grains are not equiaxed; they are slightly elongated parallel to the deformation direction. Cementite grain size in all studied alloys is about 30 nm; it confirms the estimations made using the X-ray line broadening. Their shape is more equiaxed than that of ferrite grains. Fe_3C grains are more or less uniformly distributed over the specimen. The spacing between cementite particles decreases with increasing carbon content. It is about 50–100 nm in Fe–0.3 wt.% C alloy and about 10–50 nm in the Fe–1.7 wt.% C alloy. Only two phases, namely α-Fe and Fe_3C are present after HPT in all studied alloys. No signs of retained cementite, graphite or other iron carbides are present in the SAED patterns.

Fig. 2 shows the dependence of saturation magnetization J_s on carbon concentration. Saturation magnetization decreases with increasing carbon concentration for all studied samples. All experimental points are very close to the straight line connecting the saturation values for pure Fe ($J_s = 2.16$ T [16]) and Fe_3C ($J_s = 1.24$ T [17]). However, J_s for the HPT alloys decreases with increasing carbon content slower than that of as-cast alloys. In turn, J_s for the as-cast alloys decreases with increasing carbon content slower than that of coarse-grained alloys annealed at 725 °C for 950 h. The dependence of a $\mu_0 H_c$ product (H_c is the coercivity and μ_0 is the permeability of free space) on carbon concentration was measured in [13]. The coercivity of nanostructured samples after HPT is higher than that of coarse-grained as-cast alloys. The $\mu_0 H_c$ value of hypoeutectoid as-cast alloys increases almost linearly with carbon content. In the concentration interval between 0.6 and 1.7 wt.% C, $\mu_0 H_c$ remains almost constant [13].

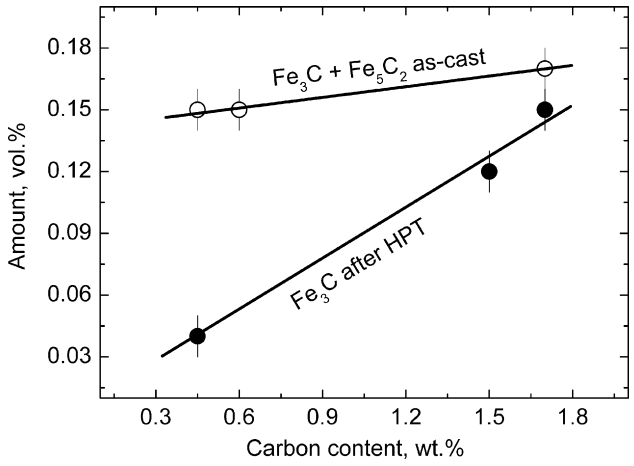

Fig. 3. Amount of iron carbides before and after HPT in dependence on carbon content based on Mössbauer measurements.

Mössbauer spectra of the as-cast alloys contain the lines of ferrite (H_{eff} = 330 kOe [18]), Hägg carbide χ-Fe_5C_2 with hyperfine fields of 185 ± 3 [19], cementite Fe_3C (H_{eff} = 210 ± 5 kOe [18]) and retained austenite (no hyperfine field) [18]. The Mössbauer spectra after HPT contain only the lines of ferrite (H_{eff} = 330 kOe [18]), and cementite Fe_3C (H_{eff} = 210 kOe). Retained austenite and Hägg carbide disappeared after HPT. Other iron carbides like ε-Fe_2C with hyperfine fields of 170 ± 3, 237 ± 3 and 130 ± 6 kOe [20,21], Fe_4C or Fe_6C were not observed either before or after HPT. This fact supports the data of XRD and TEM. In Fig. 3 the amount of carbides before HPT (Fe_3C and χ-Fe_5C_2) and after HPT (Fe_3C) is shown in dependence on carbon content (data are based on Mössbauer measurements). The amount of carbides before and after HPT increases linearly with increasing carbon content. However, the points for the as-cast Fe–C alloys lie much higher than those for the HPT alloys. This indicates decrease of the cementite amount after HPT. The samples after HPT became rather brittle, which made it possible to break them *in situ* in the Auger spectrometer chamber. The carbon concentration along GB fracture surfaces fluctuates between 10 and 70 wt.% in the layer of about 1–3 nm thickness. It reveals the strong grain boundary carbon adsorption, but not the continuous cementite GB layers.

4. Discussion

In the 1990s the nanocrystalline materials started to be produced by various methods. Later it became clear that various synthesis methods are crucially different and lead to very different structures and phase compositions of nanomaterials. The experiments on the ball milling of Fe–C alloys (steels) unambiguously showed that cementite can completely disappear from the ferrite-cementite structure after a long milling [1,2,5–7,22,23]. As a result, a non-equilibrium supersaturated solid solution of carbon in α-Fe was formed. In an early work on SPD deformation of Fe–C alloys Korznikov et al. [24] observed the disappearance of the cementite peaks from XRD spectra and assumed that, similar to the ball milling, SPD leads to the formation of the supersaturated carbon solid solution in α-Fe. The assumption that cementite disappeared from steels after HPT in [9,24] was also based on the temperature dependence of magnetization J_s (pearlitic UIC 860 V steel with 0.6–0.8 wt.% C [9] and high-carbon steel with 1.2 wt.% C [24] were studied). In the coarse-grained α-Fe + Fe_3C alloys the input of cementite into the $J_s(T)$ dependence can be clearly seen, and the derivative break at 210 °C can be observed quite well. The Curie temperature of cementite (210 °C) is lower than that of α-Fe (770 °C). However, by increasing number of anvil rotations by HPT (i.e. with decreasing grain size), the Fe_3C input into $J_s(T)$ curve flattened and disappeared. The first hypothesis of the authors [9,24] was that cementite dilutes and disappears during HPT, although neither the carbon-supersaturated ferrite nor martensite was observed in the samples. Later the same authors found by careful electron diffraction studies that cementite is present after HPT, but the Fe_3C lamellae are broken into very fine particles [7,25]. These extremely fine (few nanometers) Fe_3C particles were not detected before by conventional TEM and low-statistics XRD analysis [9,24]. Cementite becomes paramagnetic close to 210 °C. It is good visible in the $J_s(T)$ curve when the cementite forms large lamellae or particles. Yet, with increasing number of anvil rotations by HPT, the size of the cementite particles decreases drastically. The magnetic field caused by surrounding ferromagnetic α-Fe penetrates into paramagnetic Fe_3C to a certain depth and magnetizes it. This depth can be roughly estimated by the thickness of the domain wall. It is about 40 nm for α-Fe [16]. When the size of cementite particles decreases below a few dozens of nanometers, they are fully magnetized by the surrounding α-Fe, and the input of Fe_3C into $J_s(T)$ curve flattens. The refinement of cementite lamellae to very fine particles was observed also in another mode of SPD, namely by deep drawing of steel wires with a true strain above 4 [6,26,27]. Also in this case neither cementite disappeared from the steel nor was it diluted in the matrix. Later, when using the field ion microscopy, carbon atoms from the "disappeared" cementite were found to segregate in the ferrite cell and GBs [28].

In the case of Fe–C alloys, ferrite and graphite are equilibrium phases at room temperature. However, cementite becomes equilibrium at rather low pressures (0.1–0.5 GPa, depending on the temperature [29]). In our case the pressure during HPT was much higher, 5 GPa, ensuring the thermodynamic stability of cementite. Other iron carbides become stable above 5 GPa. For example, ε-carbide Fe_7C_3 becomes stable above 5.9 GPa [30]. Therefore, such carbides do not appear in our alloys after HPT. However, it may be the reason why the HPT of the U13 steel containing 1.37 wt.% C at 12 GPa resulted in appearance of ε-carbide Fe_7C_3 and Hägg carbide Fe_5C_2 at the cost of cementite [8].

The results of this work, as well as our previous data on HPT of Al-based alloys [3,4], demonstrate that HPT or deep drawing lead simultaneously to (a) the formation of a highly non-equilibrium nanometer grain structure and (b) the disappearance of non-equilibrium phases and the formation of phases which are in equilibrium at the HPT temperature and pressure. The careful experiments and analysis of previous publications on HPT demonstrate that this deformation mode leads to the grain refinement but cannot lead to the disappearance of equilibrium phases (e.g. dissolution of cementite) or formation of non-equilibrium ones (ε or Hägg iron carbides). This is the most important difference between HPT and ball milling, as two technologies for manufacturing nanostructured materials.

Most probably, the grain boundary segregation of carbon is responsible for the apparent disappearance of cementite after HPT. The grain refinement leads to the drastic increase of GB area. Carbon concentration in GBs (up to 40% C) is much higher than in the bulk of ferrite or cementite. As a result, the carbon is consumed by GB segregation layers and amount of bulk cementite decreases. The conventional XRD methods or magnetic measurements do not detect the GB layers, and reveal the apparent (full or partial) disappearance of cementite after HPT.

5. Conclusions

(i) Severe plastic deformation of Fe–C alloys by high-pressure torsion leads to the disappearance of the non-equilibrium

(metastable) phases and to the formation of the phases which are equilibrium at temperature and pressure of HPT treatment. It is an important difference from the ball milling which can lead, similar to the ion implantation, to the formation of metastable or amorphous phases.

(ii) HPT leads to the grain refinement. Carbon strongly segregates in the numerous ferrite GBs. Consumption of carbon by these GB segregation layers causes of the bulk cementite amount to decrease.

Acknowledgements

The authors thank the Russian Foundation for Basic Research (contracts 06-03-32875 and 08-08-91302) and INTELS Foundation for Science and Education (contract G-58-08-02). They also greatly appreciate Dr. U. Welzel, Dr. A. Nekrasov and Prof. R. Valiev for the fruitful discussions.

References

[1] X. Amils, J. Nogués, S. Suriñach, J.S. Muños, M.D. Baró, A. Hernando, J.P. Morniroli, Phys. Rev. B 63 (2001) 052402.
[2] L. Del Bianco, A. Hernando, E. Bonetti, E. Navarro, Phys. Rev. B 56 (1997) 8894–8901.
[3] B.B. Straumal, B. Baretzky, A.A. Mazilkin, F. Phillipp, O.A. Kogtenkova, M.N. Volkov, R.Z. Valiev, Acta Mater. 52 (2004) 4469–4478.
[4] A.A. Mazilkin, B.B. Straumal, E. Rabkin, B. Baretzky, S. Enders, S.G. Protasova, O.A. Kogtenkova, R.Z. Valiev, Acta Mater. 54 (2006) 3933–3939.
[5] M. Li, R. Birringer, W. Johnson, Nanostruct. Mater. 3 (1993) 407–412.
[6] H.G. Read, W.T. Reynolds Jr., K. Hono, T. Tarui, Scripta Mater. 37 (1997) 1221–1230.
[7] Yu. Ivanisenko, I. MacLaren, X. Sauvage, R. Valiev, H.-J. Fecht, Acta Mater. 54 (2006) 1659–1669.
[8] V.A. Shabashov, L.G. Korshunov, A.G. Mukoseev, V.V. Sagaradze, A.V. Makarov, V.P. Pilyugin, S.I. Novikov, N.F. Vildanova, Mater. Sci. Eng. A 346 (2003) 196–207.
[9] Yu. Ivanisenko, W. Lojkovski, R.Z. Valiev, H.-J. Fecht, Acta Mater. 51 (2003) 5555–5570.
[10] D. Thomas, J. Sci. Instrum. 25 (1948) 440–444.
[11] M. Hasebe, H. Ohtani, T. Nishizawa, Metal Trans. A 16 (1985) 913.
[12] G. Williamson, R. Smallman, Acta Cryst. 6 (1953) 361–363.
[13] G. Protasova, B.B. Straumal, S.V. Dobatkin, D. Goll, G. Schütz, B. Baretzky, A.A. Mazilkin, A.N. Nekrasov, J. Mater. Sci. 43 (2008) 3775–3781.
[14] A. Mazilkin, B. Straumal, S. Protasova, S. Dobatkin, B. Baretzky, J. Mater. Sci. 43 (2008) 3800–3805.
[15] T. Massalski (Ed.), Binary Alloy Phase Diagrams, ASM International, Materials Park, OH, USA, 1993.
[16] S. Chikazumi, Physics of Ferromagnetism, Clarendon Press, Oxford, 1997.
[17] American Institute of Physics, American Institute of Physics Handbook, McGraw Hill, New York, Toronto, London, 1963.
[18] V. Litvinov, Mössbauer Spectroscopy of Fe Based Alloys, Metallurgy, Moscow, 1978, in Russian.
[19] G. Le Caer, J. Dubois, J. Senateur, J. Sol. State. Chem. 19 (1976) 19.
[20] R. Arents, Yu. Maksimov, I. Suzdalev, V. Imshennik, Yu. Krupyanskiy, Fiz. Metal. Metalloved. 36 (1973) 277.
[21] Yu. Maksimov, I. Suzdalev, R. Arents, S. Loktev, Kinet. Katal. 15 (1974) 1293.
[22] S. Ohsaki, K. Hono, H. Hidaka, S. Takaki, Scripta Mater. 52 (2005) 271–276.
[23] E. Bauer-Grosse, G. Le Caer, Phil. Mag. B 56 (1987) 485–500.
[24] A.V. Korznikov, Yu.V. Ivanisenko, D.V. Laptionok, I.M. Safarov, V.P. Pilyugin, R.Z. Valiev, Nanostruc. Mater. 4 (1994) 159–167.
[25] Yu. Ivanisenko, I. MacLaren, R. Valiev, H.-J. Fecht, Adv. Eng. Mater. 7 (2005) 1011–1014.
[26] Y. Tomota, T. Suzuki, A. Kanie, Y. Shiota, M. Uno, A. Moriai, N. Minakawa, Y. Morii, Acta Mater. 53 (2005) 463–467.
[27] K. Makii, H. Yaguchi, M. Kaiso, N. Ibaraki, Y. Myamoto, Y. Oki, Scripta Mater. 37 (1997) 1753–1759.
[28] X. Sauvage, Yu. Ivanisenko, J. Mater. Sci. 42 (2007) 1615.
[29] T. Ershova, E. Ponyatovskii, Dokl. Chem. Proc. Acad. Sci. USSR 151 (1963) 724.
[30] S. Ramos, L. Amarai, M. Behar, G. Marest, A. Vasques, F. Zawislak, Radiat. Eff. Def. Sol. 110 (1989) 355.